Final Draft
of the original manuscript:

Rahman, M.M.; Shishatskiy, S.; Abetz, C.; Georgopanos, P.; Neumann, S.; Khan, M.M.; Filiz, V.; Abetz, V.:

Influence of temperature upon properties of tailor-made PEBAX® MH 1657 nanocomposite membranes for post-combustion CO2 capture

In: Journal of Membrane Science (2014) Elsevier

DOI: 10.1016/j.memsci.2014.06.048

Influence of temperature upon properties of tailor made PEBAX® MH 1657 nanocomposite membranes for post combustion CO_2 capture

Md. Mushfequr Rahman[1], Sergey Shishatskiy[1], Clarissa Abetz[1], Prokopios Georgopanos[1], Silvio Neumann[1], Muntazim Munir Khan[1], Volkan Filiz[1]*, Volker Abetz[1,2]*

[1]Helmholtz-Zentrum Geesthacht, Institute of Polymer Research, Max-Planck-Straße 1, 21502 Geesthacht, Germany

[2]University of Hamburg, Institute of Physical Chemistry, Grindelallee 117, 20146 Hamburg, Germany

Corresponding Email: volkan.filiz@hzg.de, volker.abetz@hzg.de

Abstract:

Tailor made block copolymer nanocomposite membranes are prepared by incorporation of 40 wt% methoxy poly(ethylene glycol) (PEG) functionalized polyoctahedral oligomeric silsesquioxanes (POSS) nanoparticles in commercial thermoplastic elastomer multiblock copolymer PEBAX® MH 1657. Atomic force microscopy was used to find out the location of the nanoparticles in the block copolymer matrix. Separation of CO_2 from N_2 and H_2 is studied by measurements of single gas transport properties of nanocomposite materials using the time-lag method in the temperature range 30 °C to 70

°C. PEG functionlized POSS nanoparticles increase the CO_2 permeability of the nanocomposite membranes without loss of CO_2/N_2 and CO_2/H_2 selectivity. Thermal properties of the nanocomposite membranes are studied by differential scanning calorimetry (DSC) to assess the stability of the nanocomposite membranes upon melting of polyether and polyamide blocks.

Keywords: PEBAX, POSS, Nanocomposite, Gas separation membrane.

Highlights:

- We examine PEBAX® MH 1657 nanocomposite membranes for post combustion carbon capture
- Location of nanofillers in phase separated block copolymer matrix PEBAX® MH 1657
- CO_2 separation performanceof the membranes in the temperature range 30 ºC to 70 ºC
- Structure-property relationship of the CO_2 separation membranes
- Stability of the membranes upon melting of polyether and polyamide block

1. Introduction

One of the biggest challenges to ensure sustainable industrial growth and to mitigate the climate change is to find an economically feasible separation technology for removal of CO_2 from the effluent flue gas streams. Economically, the advantage of membrane gas separation technology is immense. Simple process design and lower energy requirement compared to the conventional gas separation technologies (e.g. liquid adsorption) have

paved the way for use of the membrane technology in commercial CO_2 removal applications. [1] Large scale industries e.g. fossil fuel power plants, oil refineries, steel mills emit enormous amount of CO_2. Fossil fuel power plants alone are responsible for approximately 40% of total CO_2 emission, coal fired plants being the main contributor. [2] CO_2 selective membranes can offer a cost effective post combustion gas stream treatment process to lower the CO_2 emission of existing and future fossil fuel based power plants. In an average a 600 MW coal fired power plant generates 500 m^3/s of flue gas. In a typical coal fired power plant, the flue gas after leaving the boiler is passed through an electrostatic precipitator (to remove particulates), a desulfurizer (to remove SO_2 gas), and then CO_2 can be separated. At this stage the water saturated flue gas is at about 50°C, nearly atmospheric pressure and has a CO_2 content as low as 10-15% or CO_2 partial pressure of 100-150 mbar. [3] For this particular application the membrane must compensate the low driving force of separation with high CO_2 permeability and moderate selectivity over other gases. [4] Hence, there is an emerging research impetus to increase the permeability of the CO_2 selective polymers at the operating conditions of the power plant stack. Incorporation of nanofillers in polymer matrix resulting in formation of nanocomposite or mixed matrix membranes is a facile and efficient way towards this endeavor. Nanocomposite membranes can be prepared by physical blending [5-8] or chemical crosslinking [9, 10] with nanosized fillers.

Gas transport through a dense polymeric membrane follows the solution-diffusion mechanism. According to this mechanism, the penetrants (i.e. permeating gas molecules) are adsorbed at the feed side of the membrane, then diffuse across membrane and finally

desorb from the permeate side of the membrane. Permeability of a gas is a characteristic parameter for the membrane material which depends on the solubility and the diffusion coefficient of the penetrant in the polymeric membranes. [11, 12] Properties of both the penetrant and the polymer determine the transport of gases through the membrane. Small penetrant size, high polymer chain flexibility or high polymer fractional free volume and small polymer-penetrant interaction lead to enhanced gas diffusivity. On the other hand, strong polymer-penetrant interaction and high penetrant condensability increase the solubility. [13] Additionally, in polymer nanocomposite membranes interaction between the surface of the nanofiller with the surrounding polymer chains as well as with the permeating gases contributes to the gas transport to a great extent. Hence, one of the biggest concerns in nanocomposite membrane preparation is to decorate the surface of the nanoparticle with suitable functional group by covalent or non-covalent functionalization. Surface functionality of the nanofillers not only contributes to achieve homogeneous dispersion, but also creates an opportunity to tune the transport of penetrants through the membrane. [14, 15]

Advances in synthesis and functionalization of nanofillers have opened up a myriad of opportunities for tailoring the properties of traditional polymeric materials. However, in a block copolymer-nanoparticle composite the control of nanostructure and localization of nanoparticle as well as the fundamental understanding of structure-property relationship remains a challenge. The final morphology of the block copolymer nanocomposite is determined by a complex interplay of polymer conformational entropy, translational entropy of the nanoparticle and enthalpic interactions between the block copolymer

segment and surface functional group of the nanoparticle. Hence, it is essential to explore new methods and develop a fundamental understanding to exploit this interplay in order to design novel functional materials. [16-18]

Commercially available multiblock copolymers of the PEBAX® series consisting of an alternating sequence of flexible polyether and rigid polyamide blocks have already carved out a reputation as an appropriate choice for CO_2 separation membranes. Several studies on the structure and the gas transport properties of this block copolymer series have been reported. [19-22] Researchers have also tried to further explore the gas transport property of PEBAX® based gas separation membranes by incorporation of numerous fillers. [4, 15, 23-29] In a previous work, we have reported that PEG functionalized POSS nanoparticle is a suitable nanofiller to improve the commercial viability of block copolymer membranes containing poly(ethylene oxide) segments. [30, 31] Moreover, we have also reported PEG functionalized POSS nanoparticle containing an additional functionality can improve CO_2 separation property of PEBAX® MH 1657 membrane. [32] In this paper we discuss the influence of elevated temperature upon CO_2 separation and stability of the PEBAX® MH 1657 nanocomposite membranes containing 40wt% nanofiller aiming for post combustion carbon capture application.

2. Experimental part:

2.1. Materials:

PEBAX® MH 1657 was purchased from ARKEMA. Glycidyl POSS® and glycidyldimethylsilyl POSS® were purchased from Hybrid Plastics®. Methoxy poly(ethylene glycol) (PEG) (M_n = 350 g/mol) was purchased from Sigma-Aldrich®. All the solvents – chloroform, toluene, tetrahydrofuran and ethanol are purchased from Merck KGaA.

2.2. Membrane preparation:

The synthesized PEG modified POSS nanofillers were incorporated in PEBAX® MH 1657 (Arkema) via solution casting method. The nanofiller content was 40 wt% with respect to the final composition of the nanocomposite. 3 wt% solutions of mixture of polymer and filler were prepared in a mixture of ethanol/water (70/30 wt %) under reflux (80 °C) for 2h. The obtained homogeneous solution was cooled down to room temperature and poured into Teflon molds. Nanocomposite membranes were obtained by drying the solution at 40ºC for 24 hours. The thickness of the membranes was measured by a digital micrometer.

2.3. Characterization:

A Veeco MultiMode NanoScope IV atomic force microscope (AFM) operating in TappingMode™ was used to investigate the cross sections of the membranes at room

temperature. Cross sections were prepared under cryogenic conditions with a Leica Cryo-Ultramicrotome EM UCT FCS equipped with a diamond knife.

A Zeiss “Merlin” scanning electron microscope (SEM) was applied to analyse the surface and cross section morphologies of the PEBAX® based membranes at an accelerating voltage of 900V. With an energy selective backscattered (EsB) incolumn detector smallest differences in material composition of the membranes could be identified.

A DSC 1 (Star system) from Mettler Toledo was used to study the effect of incorporation of nanofillers upon thermal transitions of PEBAX® MH 1657 in the temperature range from -100 ºC to 250 ºC at the scan rate of 10 K/min using nitrogen as a purge gas stream (60 mL/min).

Single gas permeability, diffusion and solubility coefficients of N_2, H_2 and CO_2 were determined within the temperature range 30 ºC to 70 ºC via the constant volume, variable pressure (“time-lag”) method. The feed pressure was 1 bar for all the gases. The following equations were used to determine gas permeability (P), diffusion coefficient (D), solubility (S) coefficients and ideal selectivity for pure gases ($\alpha_{A/B}$), respectively:

$$P = D \cdot S = \frac{V_p \cdot l}{A \cdot R \cdot T \cdot \Delta t} \ln \frac{p_f - p_{p1}}{p_f - p_{p2}} \quad (1)$$

$$D = \frac{l^2}{6\theta} \quad (2)$$

$$\alpha_{A/B} = \frac{P_A}{P_B} = \frac{D_A}{D_B} \cdot \frac{S_A}{S_B} \quad (3)$$

where, V_p is the permeate volume, l is the membrane thickness, A is the membrane area, R is the gas constant, p_f is the feed pressure considered constant in the time range Δt, p_{p1} and p_{p2} are permeate pressures at time moment 1 and 2, Δt is the time difference between two points (1 and 2) on the pressure curve, θ is the time lag, indexes A and B relates to gases chosen for calculation of permeability, diffusion and solubility selectivities.

3. Results and discussion:

Scheme 1

Glycidyl POSS (Scheme 1a) and glycidyldimethylsilyl POSS (Scheme 1b) are successfully modified with PEG (Scheme 1c) using three different solvent (chloroform, toluene and THF) via epoxide ring opening reaction in presence of boron triflouride diethyletharate (Scheme 1d) catalyst at room temperature. A large excess of PEG is used in the reactions to make sure that the reaction proceeds to completion i.e. there is no unreacted epoxy ring left. Finally, the unreacted PEG is removed by extraction (using dicholoromethane and water). The reaction occurs via SN_2 mechanism in three of the investigated solvents. The solvent used for functionalization has a pronounced influence upon the final product of the synthesis. For discussion in this manuscript these

nanoparticles are given acronyms (listed in Table 1). When toluene is used as solvent the reaction (i.e. in PEG-GLY-POSS-Toluene and PEG-GDMS-POSS-Toluene) occurs merely by nucleophilic attack of PEG and no by product is observed. In chloroform although ca. 80% of the epoxy rings are opened by PEG, some of the epoxy rings are opened by the catalyst itself (in PEG-GLY-POSS-Chloroform and PEG-GDMS-POSS-Chloroform). Tetrahydrofuran molecules form complex with the functionalized nanoparticles when it is used as solvent (i.e. in PEG-GLY-POSS-THF and PEG-GDMS-POSS-THF). The synthesis of these nanoparticles is discussed in detail elsewhere. [32]

Table 1

3.1 Location of the nanoparticles in the prepared nanocomposite membranes via atomic force microscopy:

Figure 1

TappingMode™ atomic force microscopy was used to investigate the cross section of PEBAX® MH 1657 block copolymer membrane and its nanocomposites after incorporation of 40 wt% nanofiller. Figure 1 shows the phase image of the cross section of PEBAX® MH 1657 membrane. Microphase separation of the polyether and polyamide blocks is clearly visible in this image. The contrast of this image is attributed to the

difference in viscoelastic properties of the two blocks. The brighter areas correspond to the polyamide hard phase, while the darker areas correspond to the softer phase of polyether. Figure 2 depicts the cross section of the nanocomposite membranes. The PEG functionalized POSS nanoparticles appear as white spots in the AFM image. Introduction of functionalized POSS nanoparticles have profound influence on the morphology, since the particle loading is very high. Compared to the pure PEBAX® MH 1657, the size of the polyether domains are increased in the nanocomposites which is attributed to the decrease of total polyamide content due to incorporation of PEG functionalized POSS nanoparticles. It is evident that the nanoparticles are located in the polyether domain of the nanocomposite membranes. This corresponds to the fact that the interaction between the PEG ligands of the nanoparticles with the polyamide domain of PEBAX® MH 1657 is unfavorable, while with the polyether domain it is less incompatible or neutral. Hence the PEG ligand makes the nanoparticles compatible to the polyether domain of PEBAX® MH 1657, regardless of the presence of the dimethylsilyl spacer (in PEG-GDMS-POSS-Chloroform and PEG-GDMS-POSS-Toluene) or the THF complex (in PEG-GLY-POSS-THF and PEG-GDMS-POSS-THF). But the distribution of POSS in the polyether domain is not same in six nanocomposites. It is worth mentioning that the AFM imaging parameter had to be adjusted for optimal observation of the different phases. As a result the density of white spots in Figure 2 a - f differ from each other although in every case the nanocomposite contains 40 wt% nanofiller. A careful comparison of the cross section of nanocomposites (Figure 2) shows that the organization of the PEG domains of the nanocomposites is also different. For example, in 40wt% PEG-GDMS-POSS-THF incorporated PEBAX® MH 1657 nanocomposite (Figure2f) polyamide domains are

bigger in size and in most case completely surrounded by polyether domains. On the other hand, 40 wt% PEG-GLY-POSS-Chloroform shows a more co-continuous nature and finer distribution of polyether and polyamide domains (Figure 2a). Thus the difference in structural features of the nanoparticles has a pronounced influence upon the final morphology of the nanocomposites. These results agree well with SEM measurements of the top surfaces and cross sections of these membranes using the nanoscale compositional information available from low-loss backscattered electrons. The bright features correspond to POSS agglomerates, the dark continuous areas correspond to PEG and the dispersed light areas are polyamide (results are shown in the supplement).

Figure 2

3.2 Gas separation performance:

Figure 3

Permeability of N_2, H_2 and CO_2 versus the reciprocal of temperature in Kelvin is plotted in Figure 3. Permeability of all the gases increases sharply with the increase of temperature. The nanocomposite membranes show substantially high N_2, H_2 and CO_2 permeability coefficients compared to the pure PEBAX® MH 1657. A careful comparison of CO_2 permeabilities of the studied nanocomposites reveals that 40 wt% incorporation of PEG-GLY-POSS-Chloroform and PEG-GLY-POSS-Toluene gives similar CO_2 permeability values at all temperatures in the range from 30 ºC to 70 ºC. Compared to

these membranes, the nanocomposite membranes containing other nanofillers have significantly higher CO_2 permeability. Among them the nanocomposite membranes containing PEG-GDMS-POSS-Chloroform, PEG-GDMS-POSS-Toluene and PEG-GLY-POSS-THF show similar permeability. But the highest value of permeability is demonstrated by the one containing 40 wt% PEG-GDMS-POSS-THF. Permeability of H_2 and N_2 show a similar trend (like permeability of CO_2) after incorporation of different fillers in PEBAX® MH 1657. The observations from Figure 3 confirm that within the temperature range from 30 ºC to 70 ºC, the presence of a dimethylsilyl spacer and a THF complex both lead to higher gas permeability. The nanoparticles synthesized using chloroform and toluene as solvents have similar influence upon gas permeability when incorporated in PEBAX® MH 1657.

Figure 4

Figure 4 depicts the permeability selectivity of CO_2 over H_2 and N_2 in the temperature range of 30ºC to 70ºC. CO_2/H_2 permeability selectivity and CO_2/N_2 permeability selectivity drop significantly with the increase of temperature. It is clear that the nanofillers do not have any influence on CO_2/H_2 permeability selectivity in this temperature range. CO_2/N_2 permeability selectivity remains unchanged in PEG-GLY-POSS-Chloroform and PEG-GLY-POSS-Toluene incorporated nanocomposite membranes. At 30ºC the CO_2/N_2 permeability selectivity of the nanocomposites containing the other four fillers are lower than that of the pure PEBAX® MH 1657 membrane. But the difference in selectivity becomes narrower as the temperature increases and finally at 70ºC there is no significant difference in CO_2/N_2 permeability

selectivity between PEBAX® MH 1657 and its nanocomposites (discussed later in section 4.2).

Figure 5

In pure PEBAX® MH 1657 membrane and the nanocomposite membranes the diffusion coefficient of CO_2 shows a sharp rise as the temperature is increased from 30 °C to 70 °C (Figure 5). Meanwhile the CO_2 solubility follows a decreasing trend with increasing temperature. It is evident that the CO_2 diffusion coefficient of PEG-GLY-POSS-Chloroform and PEG-GLY-POSS-Toluene incorporated nanocomposite membranes are similar to that of pure PEBAX® MH 1657 membrane. The other fillers lead to higher values of diffusion coefficients. On the other hand, CO_2 solubility of all the nanocomposite membranes is higher than that of PEBAX® MH 1657 membrane. But the values of CO_2 solubility of different nanocomposite membranes are analogous as the error bars overlap each other. The permeability, diffusion and solubility of CO_2 are correlated with Arrhenius and Van't Hoff equations, in order to further explore the temperature dependence of CO_2 transport.

$$P = P_o \exp^{\frac{-E_P}{RT}} \quad (4)$$

$$D = D_o \exp^{\frac{-E_D}{RT}} \quad (5)$$

$$S = S_o \exp^{\frac{-\Delta H_S}{RT}} \quad (6)$$

Here, P_o, D_o and S_o are pre-exponential constants, E_P is the activation energy of permeation, E_D is the activation energy of diffusion and ΔH_S is the enthalpy of sorption. Equation 1, 4, 5 and 6 indicates that E_P is simply the sum of E_D and ΔH_S.

$$E_P = E_D + \Delta H_S \qquad (7)$$

In this study E_P was calculated from the slope of *ln P vs. 1/T* (using Equation 4), E_D was calculated from the slope of *ln D vs. 1/T* (using Equation 5) and ΔH_S from Equation 7. Comparison of E_P, E_D and ΔH_S (from Table 2) provides a fundamental guideline to understand the influence of nanofillers upon the transport behavior of CO_2 through the nanocomposite membranes. However, the determination of these parameters encounters the difficulty that in some cases the logarithmic plots do not generate completely straight lines as in the case of CO_2. A linear regression is used to calculate the slope. Therefore, the inherent error in the determination of these parameters must also be taken into account. Only significant changes of the parameters can be used to compare the influence of different structural features of the nanofillers on the CO_2 transport through the nanocomposite membranes.

Table 2

A positive value of E_P corresponds to an increase of permeability with increasing temperature. A significant drop of E_P can be noticed in the nanocomposite membranes compared to the pure polymer membrane. From Table 2 it is evident that, the lower value

of E_P in the nanocomposite membranes is largely due to the lower value of E_D. Moreover, PEG-GDMS-POSS-Chloroform, PEG-GDMS-POSS-Toluene and PEG-GDMS-POSS-THF contributed more to the drop of E_P and E_D than PEG-GLY-POSS-Chloroform, PEG-GLY-POSS-Toluene and PEG-GLY-POSS-THF, respectively. A negative value of ΔH_S is characteristic for decrease of sorption with increase of temperature. However, it is clear from Table 2 that the values of ΔH_S are too close to each other to make any comparison about the sorption environment of the CO_2 molecule in presence of different fillers but for all studied fillers the ΔH_s values never exceed that of pure PEBAX® MH 1657.

3.3 Differential scanning calorimetry:

Table 3

Glass transition temperature (T_g) of the polyether blocks of PEBAX® MH 1657, the nanofillers and the nanocomposites are tabulated in Table 3. The PEG ligands of the nanofillers have lower T_g compared to the polyether segments of PEBAX® MH 1657. It implies that the mobility of the PEG ligands are higher compared to the polyether segments of PEBAX® MH 1657. T_g of the polyether segment of the nanocomposites are lower compared to that of PEBAX® MH 1657. Since the nanofillers are located in the polyether domain (section 3.1) and the T_g of the blocks of PEBAX® MH 1657 decreases after incorporation of the nanofillers it is evidenet that the PEG ligand of the nanofillers plasticizes the polyether segments of PEBAX® MH 1657. Moreover, the glass transition temperatures of PEG-GDMS-POSS-Chloroform and PEG-GDMS-POSS-Toluene are

significantly lower than those of PEG-GLY-POSS-Chloroform and PEG-GLY-POSS-Toluene. Interestingly, PEG-GLY-POSS-THF and PEG-GDMS-POSS-THF exhibit lower glass transition temperatures than the other nanoparticles. The nanocomposite membranes show lower T_g compared to PEBAX® MH 1657. The decrease of T_g is more significant for nanocomposites containing PEG-GDMS-POSS-Chloroform, PEG-GDMS-POSS-Toluene and PEG-GLY-POSS-THF, compared to PEG-GLY-POSS-Chloroform and PEG-GLY-POSS-Toluene containing nanocomposites (discussed later in section 4.1). In case of PEG-GDMS-POSS-THF incorporated nanocomposite the T_g is not clearly visible.

Figure 6

To investigate the melting and crystallization behavior of the functionalized nanoparticles the thermal history was erased by heating up to 100 °C and then they were cooled down to -100 °C. Figures 6a & Figure 6b show the second heating and second cooling trace of the DSC run. Except PEG-GDMS-POSS-THF the ligand attached to other synthesized nanoparticles exhibit cold crystallization on the heating cycle and do not crystallize on the cooling cycle of the DSC run. The weight of PEG ligands attached to nanoparticles is M_n=350 g/mol and is probably too small to crystallize during the cooling cycle at 10 K/min, which accounts for the cold crystallization behavior observed during heating cycle. For PEG-GDMS-POSS-Chloroform and PEG-GDMS-POSS-Toluene the onset of cold crystallization are -50 °C and -44 °C while the heat of cold crystallization are 20 J/g & 21 J/g. But for both PEG-GLY-POSS-Chloroform and PEG-GLY-POSS-Toluene the

onsets of cold crystallization are -26 °C and the heat of cold crystallization is 2 J/g. The enthalpies of crystallization are normalized to the total mass of sample on the pan. Thus on the heating cycle of the DSC run the nanoparticles containing the dimethylsilyl spacer exhibit the cold crystallization at significantly lower temperature and evolve approximately 10 times more heat per unit mass of the nanoparticle. Interestingly the onset and heat of cold crystallization of PEG-GLY-POSS-THF is -47 °C and 18J/g respectively. For PEG-GDMS-POSS-THF nanoparticle although a small trace of cold crystallization was observed during heating cycle, major portion of the crystallization starts at -33 °C already while cooling down from the melt and the heat of crystallization is 18 J/g. It is worth mentioning that third and fourth heating and cooling cycles in the temperature range -100 °C to 150 °C produce thermograms similar to the second heating & cooling cycle presented in Figure 6. Hence it is evident that the presence of dimethylsilyl spacer as well as the THF complex (in PEG-GLY-POSS-THF and PEG-GDMS-POSS-THF) facilitates the crystallization of PEG ligand.

Figure 7

Figure 7a depicts the temperature protocol of DSC runs for PEBAX® MH 1657 and its nanocomposites while Figure 7b illustrates the DSC thermogram of PEBAX® MH 1657. This temperature protocol is designed to study the influence of melting of the polyether blocks and the polyamide blocks upon the stability of nanocomposites. The sample is heated up to 100 °C (step 1) to remove the residual solvents and moisture, followed by a 5 min isotherm at 100 °C (step 2). At this stage only the polyether block of PEBAX® MH

1657 is in molten form. The crystallization of polyether block starts at -5 °C and ends at -22 °C as the sample is cooled down to -100 °C (step 3). The sample is heated to 100 °C and cooled down to -100 °C for two more times (steps 4 - 12). The cooling traces of step 7 and 11 show that while cooling down from 100 °C the exothermic peak of crystallization of polyether blocks appears at the same temperature. In step 13 the sample is heated up to 250 °C to melt both the polyether and the polyamide block. The cooling trace of step 15 shows that the crystallization exotherm of polyether blocks shifts to a lower temperature (onset -11 °C and endset -26 °C) compared to those observed in step 3, 7 and 11. The heating trace of step 17 shows that the melting endotherm of polyether blocks is slightly shifted to a lower temperature too, but the shape of the peak is unchanged. DSC thermograms of the nanocomposites (obtained using the temperature protocol presented in Figure 7a) are depicted in Figure 8. The cooling traces of step 3, 7 and 11 show that the crystallization exotherms of polyether domain are identical. Similarly in step 5, 9 and 11the melting endotherms of polyether domains are identical. Moreover, although these nanocomposites contain 40 wt% of nanofiller, no recrystallization of polyether is observed in these steps. It is evident that due to the high compatibility between the PEG ligand of the nanofillers and polyether segment of the block copolymers, they crystallize together during the cooling cycle of the DSC runs. However, compared to pure PEBAX® MH 1657 broadening of the polyether domain melting endotherms and crystallization exotherms was observed in the nanocomposites. Contrariwise, when both the polyether and the polyamide blocks are completely melted (by heating up to 250 °C in step 13), in the subsequent cooling and heating trace, i.e. step15 and step 17 substantial change is observed in the crystallization exotherm and

melting endotherm of the polyether blocks. In Figure 8 c, d and e recrystallization of PEG ligand of the nanofillers is observed prior to the melting endotherm in step 17. In Figure 8f two separate crystallization exotherms and melting endotherms are clearly visible for the PEG ligands of the nanofiller and polyether domain of the block copolymer.

Figure 8

It is evident from the DSC study that as long as the nanocomposites were heated up to 100 °C and cooled down to -100 °C to operate solely with the polyether domains, the nanocomposites were quite stable (since the melting and crystallization of the of the polyether domain remains unchanged even after three thermal cycles), but when the polyamide blocks are completely melted (by heating up to 250 °C in step 13), in the subsequent cooling step the block copolymer matrix start to reject a fraction of the nanofillers and they crystallize separately from the polymer matrix.

4. Discussion:

4.1. Influence of structural features of the nanofillers upon gas permeation:

The diffusion coefficient for a given gas molecule in amorphous or rubbery polymer membranes is related to the dynamics or mobility of the polymer chains. E_D is the energy required for a gas molecule to execute a diffusive jump. In rubbery polymers, at elevated

temperature the increase of polymer chain motion leads to the formation of transient chain gaps more frequently that enable easier penetrant diffusive jumps from one equilibrium site to another. As a result, higher temperature leads to an enhancement of the diffusion coefficient and it follows ultimately an increased permeability. This phenomenon is apparently well known and is regarded as typical for amorphous polymer membranes.[33] In the prepared nanocomposite membranes the PEG grafted nanoparticles are located in polyether domains (presented in Figure 2). Moreover, the T_g of the polyether domains of the nanocomposites are significantly lower than that of pure PEBAX® MH 1657 membrane (listed in Table 3). As T_g is a crude indicator of the mobility of polymer segments, it is evident that the mobility of polyether segments of the nanocomposites is higher than that of PEBAX® MH 1657 membrane. Additionally, higher diffusion coefficients accompanied with lower values of E_D of the nanocomposite membranes reveal that, due to the higher chain mobility the permeating CO_2 molecules experience lower resistance to diffusive jumps in the nanocomposite membranes compared to pure PEBAX® MH 1657. Besides, T_g (listed in Table 2) and E_D (listed in Table 3) values are significantly lower for the nanocomposites which contain the nanoparticles that have the dimethylsilyl spacer. These observations indicate that in studied nanocomposite membranes the mobility of the polyether segments surrounding the nanoparticles having dimethylsilyl spacer is higher compared to the nanocomposites where the nanoparticles do not have such moiety. It is well-known that the polymers containing flexible Si-O linkage in the main and side chains exhibits high gas permeability which stems from the low energy barrier of rotation of the Si-O linkage of the dimethylsilyl group.[34] In the PEG grafted nanoparticles obtained from glycidyl

POSS (Scheme 1a) and glycidyldimethlysilyl POSS (Scheme 1b) the ligands are connected to the silsesquioxane core through Si-C and Si-O bonds, respectively. For this reason, the presence of the dimethylsilyl group in between the cage structure of POSS and PEG ligand increases the flexibility of PEG ligands (discussed in section 3.3) which eventually leads to higher segmental mobility of polyether blocks of PEBAX® MH 1657 in the nanocomposite membranes. Although it is evident that the THF complex (in PEG-GLY-POSS-THF and PEG-GDMS-POSS-THF) leads to similar phenomenon, the interaction between the THF complex and polyether domain of the block copolymer is not completely clear from the results available at present.

4.2 Influence of nanofiller upon selectivity of CO_2 over N_2 and H_2:

At 30 ºC CO_2/N_2 permeability selectivity in PEBAX® MH 1657 is five times higher than that of CO_2/H_2 selectivity (Figure 4). The diffusion of CO_2 in PEBAX® MH 1657 membrane (Figure 5) is analogous to that of N_2 (supplementary information S3) and lower than that of H_2 (supplementary information S4) which becomes more obvious from a comparison of the diffusion selectivity of CO_2/H_2 and CO_2/N_2 gas pairs. At 30 ºC the CO_2/N_2 diffusion selectivity (supplementary information S3) is ca. 0.8 (i.e. close to 1) while the CO_2/H_2 diffusion selectivity is ca. 0.1 only. This phenomenon is attributed to the ratio of kinetic diameters of CO_2, N_2 and H_2. [13] But CO_2 enjoys much higher solubility in PEBAX® MH 1657 (Figure 5) membrane compared to N_2 and H_2 (supplementary information S3 and S4) which is attributed to high condensability of CO_2 and the quadrapole-dipole interaction between CO_2 and polar ether oxygen of the

membrane. [13] Therefore the relatively higher permeation of CO_2 compared to H_2 i.e. CO_2/H_2 selectivity suffers from the fact that the advantage of higher solubility of CO_2 is largely offset by higher diffusion of H_2 which leads to very low CO_2/H_2 selectivity.

In the nanocomposite membrane CO_2/H_2 permeability selectivity remains unchanged. At 30 ºC the nanocomposites containing PEG-GLY-POSS-THF, PEG-GDMS-POSS-Chloroform, PEG-GDMS-POSS-Toluene, and PEG-GDMS-POSS-THF shows slightly lower value of CO_2/N_2 permeability selectivity than PEBAX® MH 1657. Hence, the nanofillers containing the dimethylsilyl spacer and the THF complex have a small but statistically significant influence on CO_2/N_2 permeability selectivity of the nanocomposite membranes but not on CO_2/H_2 permeability selectivity. In these nanocomposite membranes the solubility of N_2 and H_2 is slightly higher and the solubility selectivity of CO_2/N_2 and CO_2/H_2 is lower compared to PEBAX® MH 1657 (supplementary information S3 to S6). This small change of solubility leads to marginal loss of CO_2/N_2 permeability selectivity at 30 ºC (as the diffusion selectivity is close to unity). On the other hand the low value of CO_2/H_2 permeability selectivity (which is highly offset by the much higher diffusion of smaller H_2 compared to that of CO_2) is not influenced by such small change of solubility.

The CO_2/N_2 permeability selectivity decreases in all the membranes with increasing temperature and follows similar trend. At elevated temperature (e.g. 70 ºC) the values of CO_2/N_2 selectivity of the membranes differ less from each other. An increase of temperature leads to higher kinetic energy of the permeating gas molecules & higher

mobility of polymer chains of the amorphous polyether block. As a result diffusion of the gases increases significantly but solubility decreases. For example, CO_2 diffusion in PEBAX® MH 1657 increases four times as the temperature is increased from 30 ºC to 70 ºC while CO_2 solubility decreases significantly (Figure 5). Hence, at elevated temperature (e.g. 70 ºC) the permeation of gas molecules are dominated more by diffusion than solubility. In these circumstances the values CO_2/N_2 selectivity of the nanocomposites and PEBAX® MH 1657 become analogous.

4.3 Influence of temperature upon stability of the membrane:

Thermoplastic elastomeric block copolymers having alternating hard and soft blocks are often considered as systems where the hard blocks (having high glass transition and melting temperature) act as virtual physical crosslinks between the soft blocks. [35, 36] In contrast to the covalently crosslinked systems, in this case at a temperature where the hard block is in a molten state this physical crosslinking does not exist anymore. From section 3.1 it is evident that when the nanocomposite membranes are prepared by a solution casting method, the PEG functionalized POSS nanoparticles are located in the polyether domains of the block copolymer nanocomposite system due to unfavorable interaction with the polyamide blocks. Since for post combustion carbon capture the application temperature is between 50 °C to 60 °C (explained in section 1), the gas permeability measurements were done between 30 °C to 70 °C (plotted in Figure 3). In this temperature range the polyether block is molten but the polyamide block remains in a crystalline state. From the DSC study in section 3.3 it is clear that the nanocomposite

membranes are quite stable in a temperature range where the polyamide block is not in a molten state. In other words, in the expected temperature range of post combustion carbon capture the physical crosslinking provided by the crystalline polyamide blocks exists and the nanoparticles are securely trapped in the amorphous polyether blocks. Once the hard block melts the physical crosslinking is destroyed and the nanocomposite obtains the possibility for reorganization of block copolymer's domains during the material cooling. In this circumstance the matrix starts to reject the nanoparticles from the polyether domains and the nanocomposites are not stable anymore. Hence, the application of nanocomposite membranes based on block copolymers with hard and soft domains is limited to a temperature range where the melting of the hard domain does not occur.

5. Conclusion:

This paper demonstrates that it is possible to regulate the gas transport through PEG functionalized POSS nanoparticle incorporated PEBAX® MH 1657 membrane by taking advantage of the flexibility of Si-O bond as a linkage between the core and the ligand of the nanoparticle. Furthermore, it shows that the THF complex (in PEG-GLY-POSS-THF and PEG-GDMS-POSS-THF) is also a useful structural feature to fabricate nanocomposite membranes. Both the dimethylsilyl spacer between the cage structure of POSS and PEG ligand and the THF complex can substantially improve the CO_2 permeability of the PEBAX® MH 1657 nanocomposite membrane without significant

loss of selectivity. This concept can be instrumental in designing next generation nanocomposite membranes for post combustion carbon capture. The operation temperature of the separation process implementing the studied block-copolymer based nanocomposite membranes is limited by the melting temperature of hard domains of the block copolymer. As the expected temperature range (50 – 60 °C) of CO_2 separation process in post combustion carbon capture technology is marginally below the melting temperature of hard block (above 100 °C) the nanocomposites presented here are suitable materials for this application.

Acknowledgment:

This work was financially supported the Helmholtz Association of German Research Centres through the Helmholtz Portfolio MEM-BRAIN.

References:

[1] R.W. Baker, Future Directions of Membrane Gas Separation Technology, Industrial & Engineering Chemistry Research, 41 (2002) 1393-1411.
[2] X. He, M.-B. Hägg, Hollow fiber carbon membranes: Investigations for CO2 capture, Journal of Membrane Science, 378 (2011) 1-9.
[3] T.C. Merkel, H. Lin, X. Wei, R. Baker, Power plant post-combustion carbon dioxide capture: An opportunity for membranes, Journal of Membrane Science, 359 (2010) 126-139.
[4] S. Shishatskiy, J.R. Pauls, S.P. Nunes, K.-V. Peinemann, Quaternary ammonium membrane materials for CO2 separation, Journal of Membrane Science, 359 (2010) 44-53.
[5] N. Hao, M. Böhning, A. Schönhals, CO2 Gas Transport Properties of Nanocomposites Based on Polyhedral Oligomeric Phenethyl-Silsesquioxanes and Poly(bisphenol A carbonate), Macromolecules, 43 (2010) 9417-9425.

[6] K. Madhavan, B.S.R. Reddy, Structure–gas transport property relationships of poly(dimethylsiloxane–urethane) nanocomposite membranes, Journal of Membrane Science, 342 (2009) 291-299.
[7] P. Iyer, G. Iyer, M. Coleman, Gas transport properties of polyimide–POSS nanocomposites, Journal of Membrane Science, 358 (2010) 26-32.
[8] H. Ríos-Dominguez, F.A. Ruiz-Treviño, R. Contreras-Reyes, A. González-Montiel, Syntheses and evaluation of gas transport properties in polystyrene–POSS membranes, Journal of Membrane Science, 271 (2006) 94-100.
[9] N.P. Patel, A.C. Miller, R.J. Spontak, Highly CO2-Permeable and Selective Polymer Nanocomposite Membranes, Advanced Materials, 15 (2003) 729-733.
[10] M.L. Chua, L. Shao, B.T. Low, Y. Xiao, T.-S. Chung, Polyetheramine–polyhedral oligomeric silsesquioxane organic–inorganic hybrid membranes for CO2/H2 and CO2/N2 separation, Journal of Membrane Science, 385–386 (2011) 40-48.
[11] E.R. Hensema, Polymeric Gas Separation Membranes, Adv. Mater., 6 (1994) 269-279.
[12] G. Maier, Gas Separation with Polymer Membranes, Angewandte Chemie International Edition, 37 (1998) 2960-2974.
[13] H. Lin, B.D. Freeman, Materials selection guidelines for membranes that remove CO2 from gas mixtures, Journal of Molecular Structure, 739 (2005) 57-74.
[14] H. Cong, M. Radosz, B.F. Towler, Y. Shen, Polymer–inorganic nanocomposite membranes for gas separation, Separation and Purification Technology, 55 (2007) 281-291.
[15] J.H. Kim, Y.M. Lee, Gas permeation properties of poly(amide-6-b-ethylene oxide)–silica hybrid membranes, Journal of Membrane Science, 193 (2001) 209-225.
[16] M.R. Bockstaller, R.A. Mickiewicz, E.L. Thomas, Block Copolymer Nanocomposites: Perspectives for Tailored Functional Materials, Advanced Materials, 17 (2005) 1331-1349.
[17] A.C. Balazs, Nanocomposites: Economy at the nanoscale, Nat Mater, 6 (2007) 94-95.
[18] A.C. Balazs, T. Emrick, T.P. Russell, Nanoparticle Polymer Composites: Where Two Small Worlds Meet, Science, 314 (2006) 1107-1110.
[19] V.I. Bondar, B.D. Freeman, I. Pinnau, Gas sorption and characterization of poly(ether-b-amide) segmented block copolymers, Journal of Polymer Science Part B: Polymer Physics, 37 (1999) 2463-2475.
[20] V.I. Bondar, B.D. Freeman, I. Pinnau, Gas transport property of poly(ether-b-amide) segmented block copolymers, Journal of Polymer Science Part B: Polymer Physics, 38 (2000) 2051-2062.
[21] J.H. Kim, S.Y. Ha, Y.M. Lee, Gas permeation of poly(amide-6-b-ethylene oxide) copolymer, Journal of Membrane Science, 190 (2001) 179-193.
[22] V. Barbi, S.S. Funari, R. Gehrke, N. Scharnagl, N. Stribeck, SAXS and the Gas Transport in Polyether-block-polyamide Copolymer Membranes, Macromolecules, 36 (2003) 749-758.
[23] R.S. Murali, S. Sridhar, T. Sankarshana, Y.V.L. Ravikumar, Gas Permeation Behavior of Pebax-1657 Nanocomposite Membrane Incorporated with Multiwalled Carbon Nanotubes, Industrial & Engineering Chemistry Research, 49 (2010) 6530-6538.

[24] B. Yu, H. Cong, Z. Li, J. Tang, X.S. Zhao, Pebax-1657 nanocomposite membranes incorporated with nanoparticles/colloids/carbon nanotubes for CO2/N2 and CO2/H2 separation, Journal of Applied Polymer Science, (2013) DOI: 10.1002/app.39500.
[25] Y. Li, T.-S. Chung, Molecular-level mixed matrix membranes comprising Pebax® and POSS for hydrogen purification via preferential CO2 removal, Int. J. Hydrogen Energy, 35 (2010) 10560-10568.
[26] A. Car, C. Stropnik, W. Yave, K.-V. Peinemannb, PEG modified poly(amide-b-ethylene oxide) membranes for CO_2 separation, J. Membr. Sci., 307 (2008) 88-95.
[27] W. Yave, A.Car, K.V. Peinemann, Nanostructure membrane material designed for carbondioxide separation, J. Membr. Sci., 350 (2010) 124-129.
[28] S.R. Reijerkerk, M.H. Knoef, K. Nijmeijer, M. Wessling, Poly(ethylene glycol) and poly(dimethyl siloxane): Combining their advantages into efficient CO2 gas separation membranes, J. Membr. Sci., 352 (2010) 126-135.
[29] J. Lillepärg, P. Georgopanos, S. Shishatskiy, Stability of blended polymeric materials for CO2 separation, Journal of Membrane Science, 467 (2014) 269-278.
[30] M.M. Rahman, V. Filiz, S. Shishatskiy, C. Abetz, S. Neumann, S. Bolmer, M.M. Khan, V. Abetz, PEBAX® with PEG functionalized POSS as nanocomposite membranes for CO2 separation, Journal of Membrane Science, 437 (2013) 286-297.
[31] M.M. Rahman, V. Filiz, S. Shishatskiy, S. Neumann, M.M. Khan, V. Abetz, PEG Functionalized POSS Incorporated PEBAX Nanocomposite Membranes, Procedia Engineering, 44 (2012) 1523-1526.
[32] M.M. Rahman, V. Filiz, M.M. Khan, B.N. Gacal, V. Abetz, Functionalization of POSS nanoparticle and fabrication of block copolymer nanocomposite membranes for CO_2 separation, Reactive and Functional Polymers, (Submitted).
[33] K. Ghosal, B.D. Freeman, Gas separation using polymer membranes: an overview, Polymers for Advanced Technologies, 5 (1994) 673-697.
[34] Y. Kawakami, I. Imae, Functionality and stereochemical design of silicon-containing polymers, Macromolecular Chemistry and Physics, 200 (1999) 1245-1256.
[35] T. Kamal, S.-Y. Park, J.-H. Park, Y.-W. Chang, Structural evolution of poly(ether-b-amide12) elastomers during the uniaxial stretching: An in situ wide-angle X-ray scattering study, Macromol. Res., 20 (2012) 725-731.
[36] J.P. Sheth, J. Xu, G.L. Wilkes, Solid state structure–property behavior of semicrystalline poly(ether-block-amide) PEBAX® thermoplastic elastomers, Polymer, 44 (2003) 743-756.
List of legends:

Scheme Caption:

Scheme 1: Structure of a) glycidyl POSS b) glycidyldimethylsilyl POSS c) methoxy poly(ethylene glycol) (PEG) d) boron triflouride diethyletharate.

Figure Captions:

Figure 1: AFM image of the cross section of a PEBAX® MH1657 membrane.

Figure 2: Cross section of nanocomposites of PEBAX MH 1657 containing 40 wt% of: - a) PEG-GLY-POSS-Chloroform b) PEG-GLY-POSS-Toluene c) PEG-GLY-POSS-THF d) PEG-GDMS-POSS-Chloroform e) PEG-GDMS-POSS-Toluene f) PEG-GDMS-POSS-THF.

Figure 3: Permeability of gases as a function of temperature of PEBAX® MH 1657 and nanocomposites containing 40 wt% nanofiller.

Figure 4: CO_2 permeability selectivity over N_2 and H_2 as a function of temperature of PEBAX® MH 1657 and nanocomposites containing 40 wt% nanofiller.

Figure 5: Solubility and diffusion coefficient of CO_2 as a function of temperature of PEBAX® MH 1657 and nanocomposites containing 40 wt% nanofiller.

Figure 6: DSC thermogram of synthesized nanofillers a) 2nd heating trace b) 2nd cooling trace.

Figure 7: a) Temperature protocol of DSC run b) DSC thermogram of PEBAX® MH 1657.

Figure 8: DSC thermogram (second cooling trace) of the nanocomposites of PEBAX® MH 1657 containing (a) PEG-GLY-POSS-Chloroform (b) PEG-GLY-POSS-Toluene (c) PEG-GLY-POSS-THF (d) PEG-GDMS-POSS-Chloroform (e) PEG-GDMS-POSS-Toluene (f) PEG-GDMS-POSS-THF.

Table captions:

Table 1: Acronyms of the products of epoxy ring opening reaction.

Table 2: Comparison of E_P, E_D and ΔH_S of CO_2 transport through nanocomposites containing different nanofillers.

Table 3: Glass transition temperature of PEBAX® MH 1657, the nanofillers and the nanocomposites.

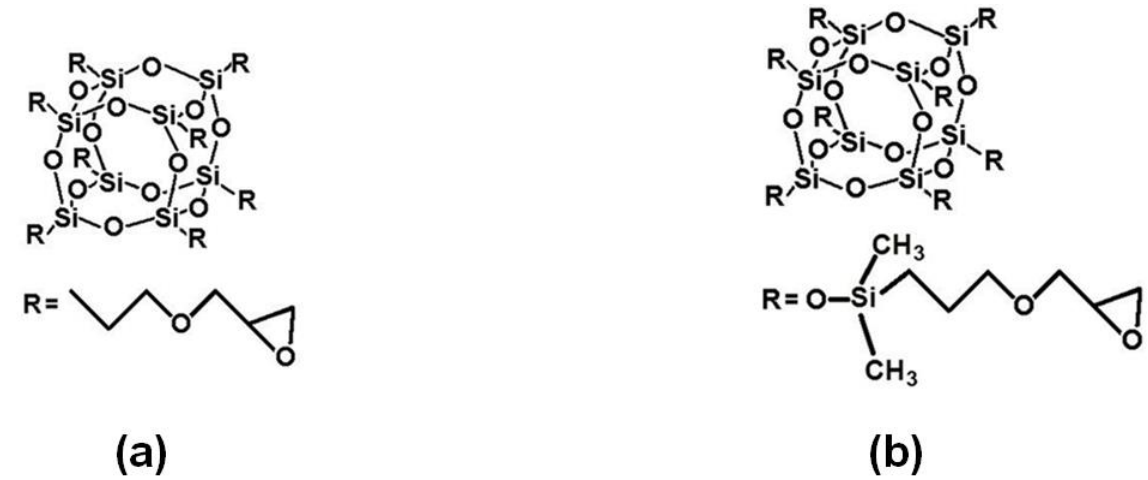

Scheme 1

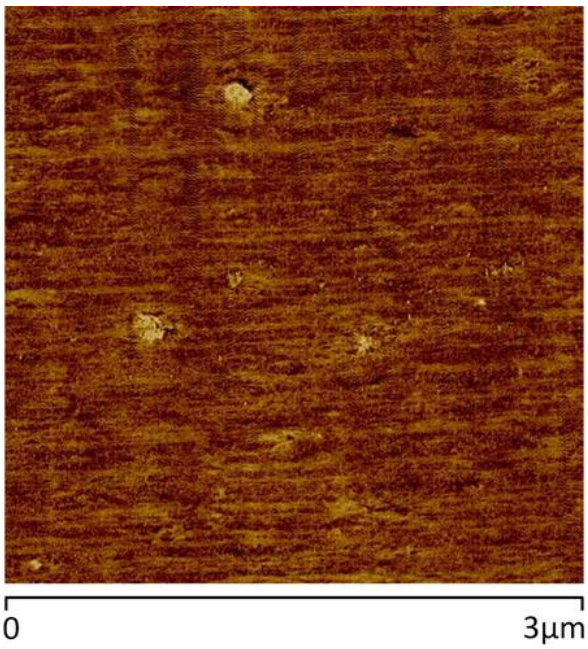

Figure 1

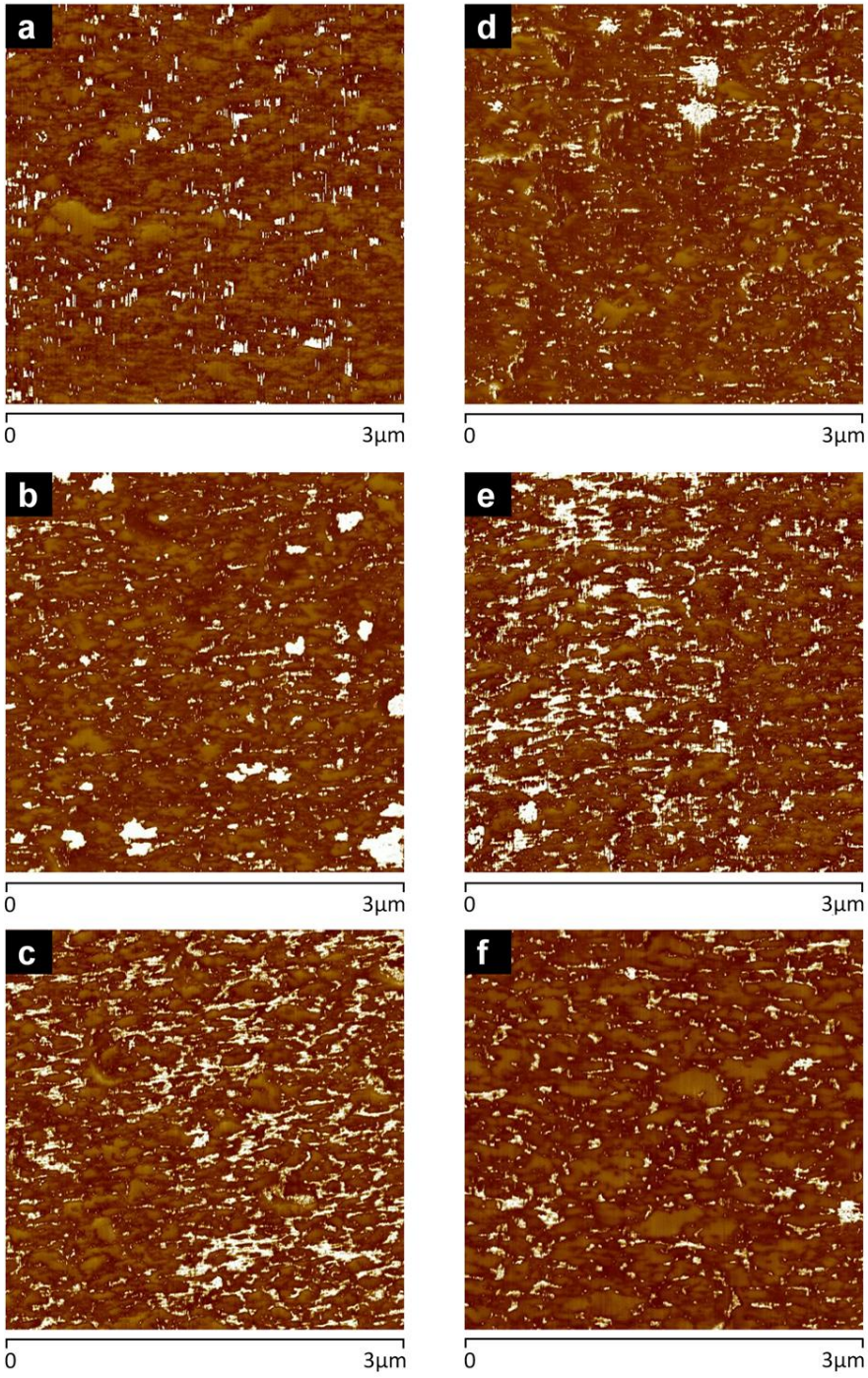

Figure 2

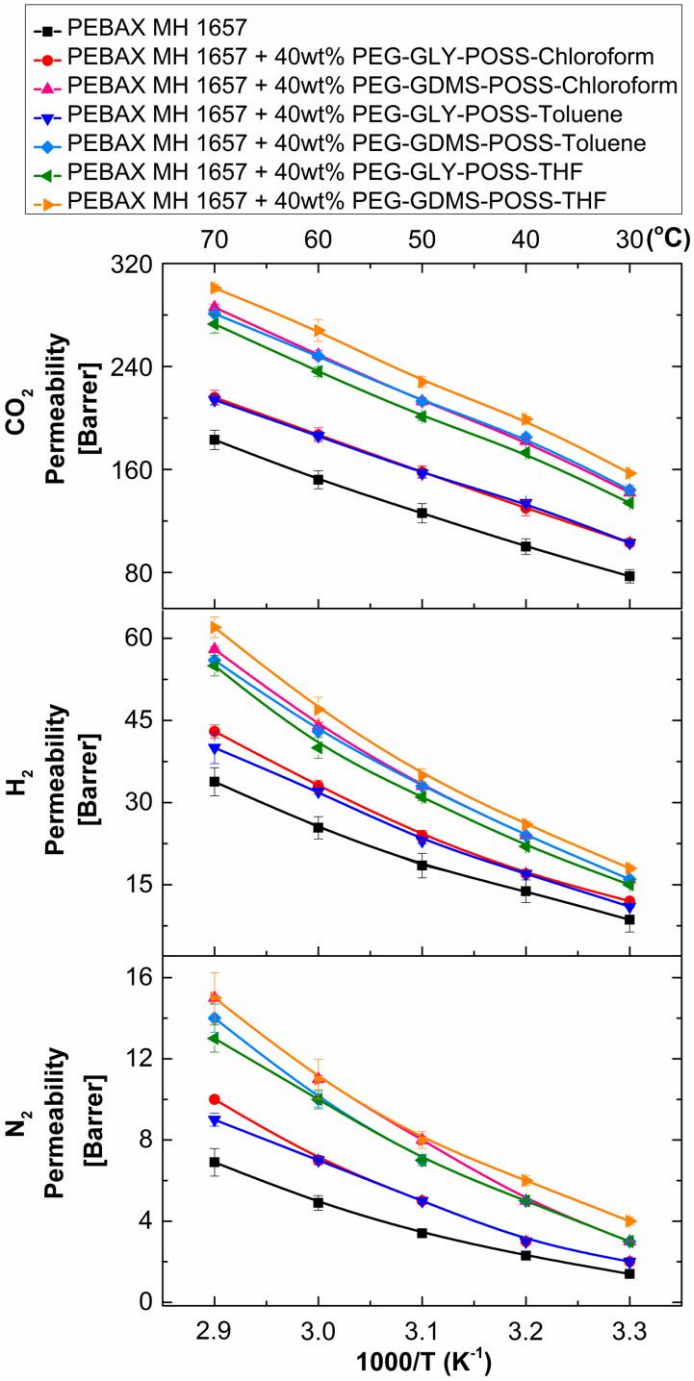
PEBAX MH 1657
PEBAX MH 1657 + 40wt% PEG-GLY-POSS-Chloroform
PEBAX MH 1657 + 40wt% PEG-GDMS-POSS-Chloroform
PEBAX MH 1657 + 40wt% PEG-GLY-POSS-Toluene
PEBAX MH 1657 + 40wt% PEG-GDMS-POSS-Toluene
PEBAX MH 1657 + 40wt% PEG-GLY-POSS-THF
PEBAX MH 1657 + 40wt% PEG-GDMS-POSS-THF
70
60
50
40
30(°C)
CO2 Permeability [Barrer]
320
240
160
80
H2 Permeability [Barrer]
60
45
30
15
N2 Permeability [Barrer]
16
12
8
4
0
2.9
3.0
3.1
3.2
3.3
1000/T (K-1)

Figure 3

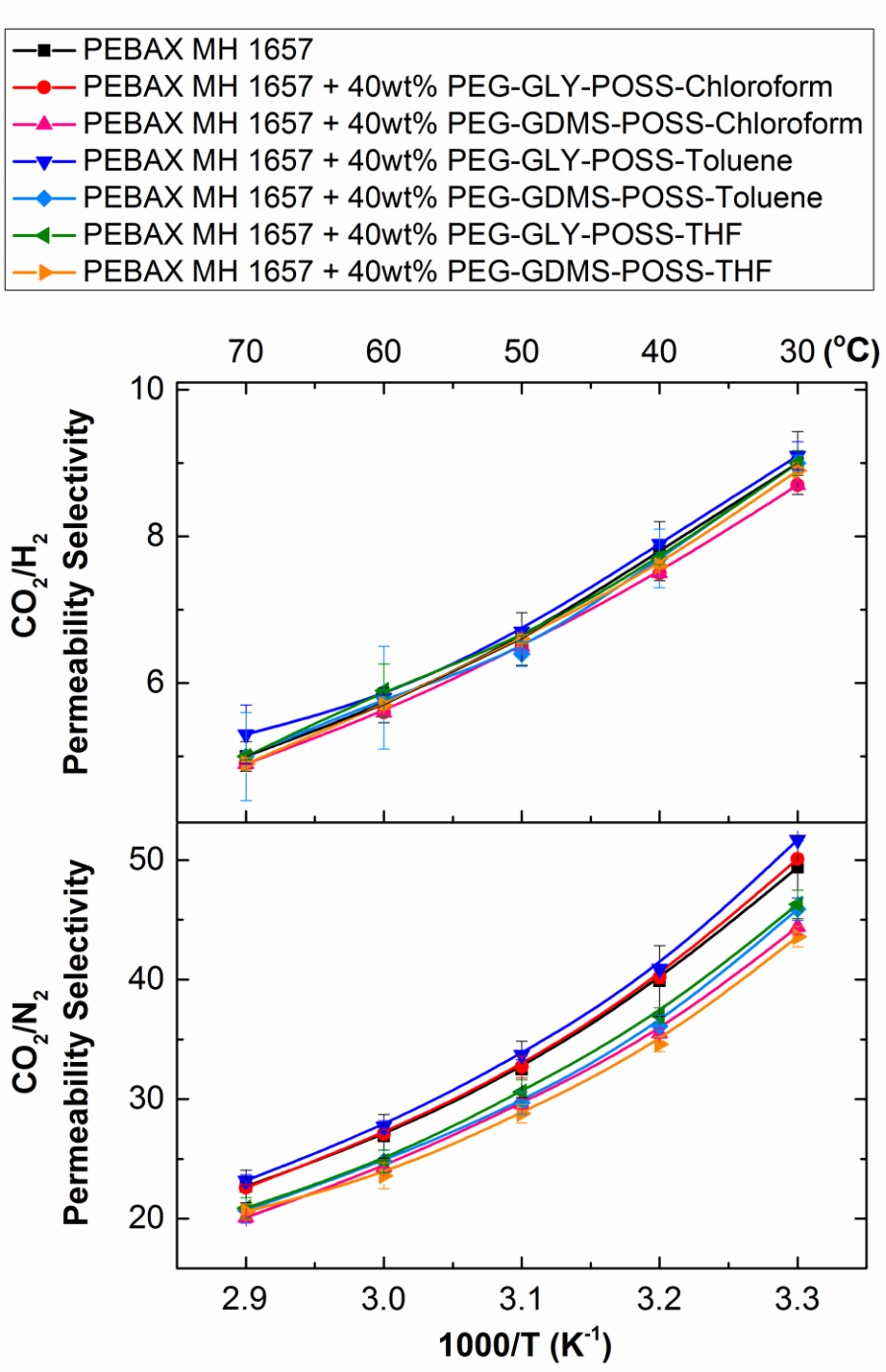
PEBAX MH 1657
PEBAX MH 1657 + 40wt% PEG-GLY-POSS-Chloroform
PEBAX MH 1657 + 40wt% PEG-GDMS-POSS-Chloroform
PEBAX MH 1657 + 40wt% PEG-GLY-POSS-Toluene
PEBAX MH 1657 + 40wt% PEG-GDMS-POSS-Toluene
PEBAX MH 1657 + 40wt% PEG-GLY-POSS-THF
PEBAX MH 1657 + 40wt% PEG-GDMS-POSS-THF
70
60
50
40
30 (°C)
CO2/H2 Permeability Selectivity
10
8
6
CO2/N2 Permeability Selectivity
50
40
30
20
2.9
3.0
3.1
3.2
3.3
1000/T (K-1)

Figure 4

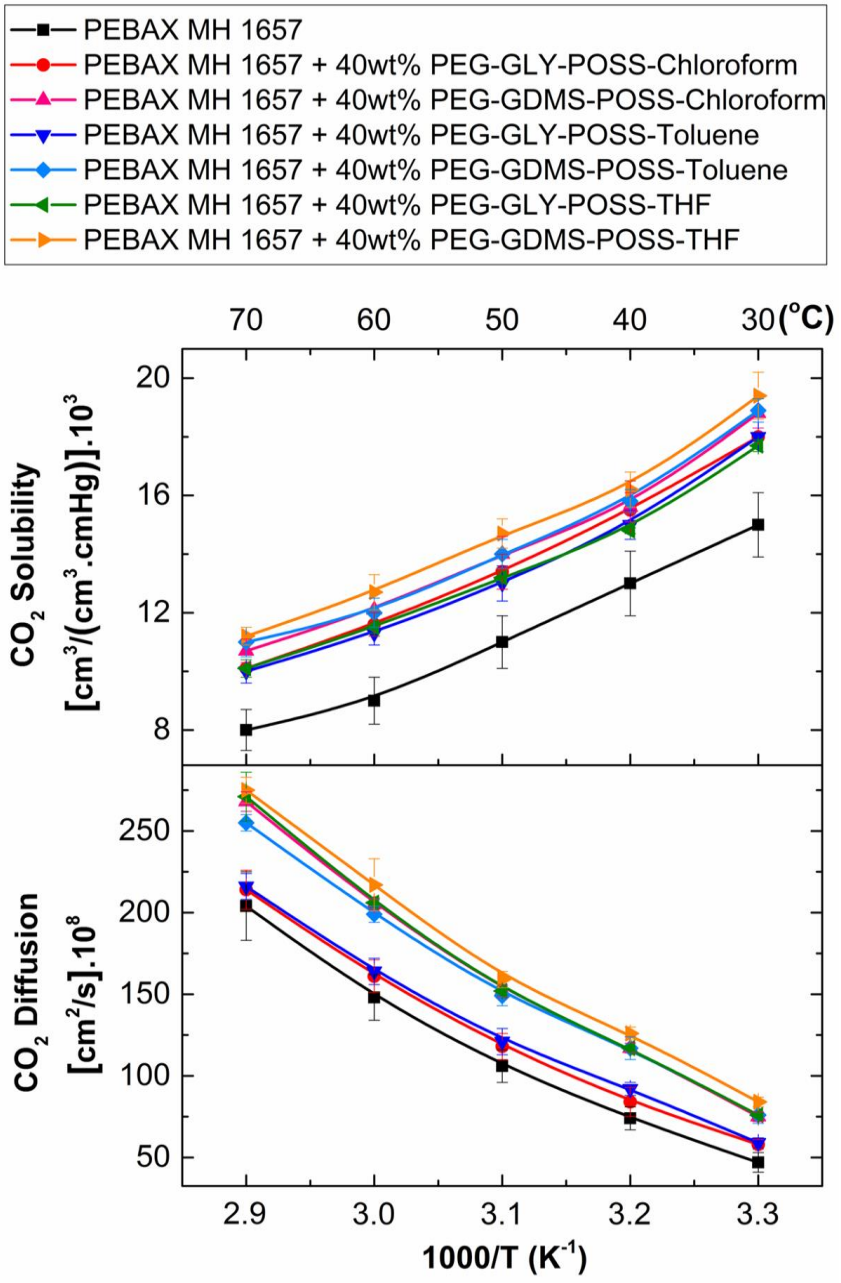
PEBAX MH 1657
PEBAX MH 1657 + 40wt% PEG-GLY-POSS-Chloroform
PEBAX MH 1657 + 40wt% PEG-GDMS-POSS-Chloroform
PEBAX MH 1657 + 40wt% PEG-GLY-POSS-Toluene
PEBAX MH 1657 + 40wt% PEG-GDMS-POSS-Toluene
PEBAX MH 1657 + 40wt% PEG-GLY-POSS-THF
PEBAX MH 1657 + 40wt% PEG-GDMS-POSS-THF
70
60
50
40
30(°C)
CO2 Solubility
[cm3/(cm3.cmHg)].10^3
20
16
12
8
CO2 Diffusion
[cm2/s].10^8
250
200
150
100
50
2.9
3.0
3.1
3.2
3.3
1000/T (K-1)

Figure 5

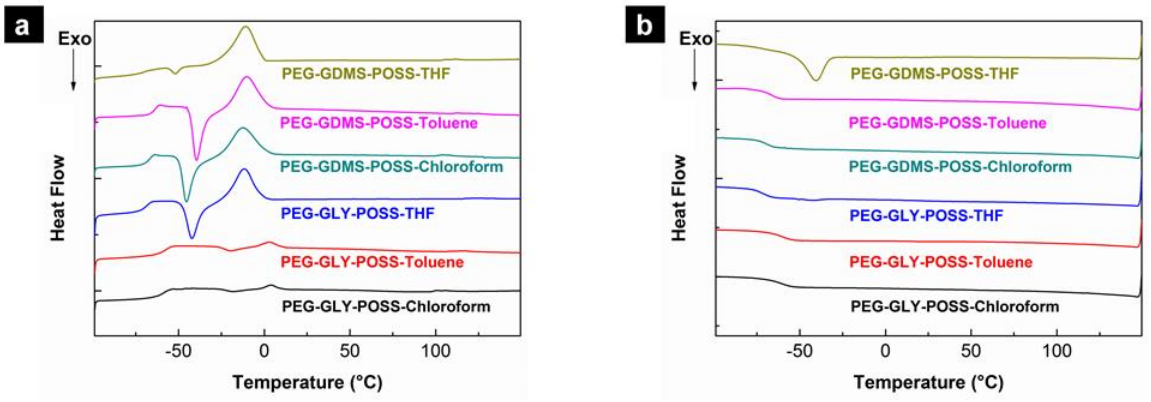
a
Exo
Heat Flow
PEG-GDMS-POSS-THF
PEG-GDMS-POSS-Toluene
PEG-GDMS-POSS-Chloroform
PEG-GLY-POSS-THF
PEG-GLY-POSS-Toluene
PEG-GLY-POSS-Chloroform
-50
0
50
100
Temperature (°C)
b
Exo
Heat Flow
PEG-GDMS-POSS-THF
PEG-GDMS-POSS-Toluene
PEG-GDMS-POSS-Chloroform
PEG-GLY-POSS-THF
PEG-GLY-POSS-Toluene
PEG-GLY-POSS-Chloroform
-50
0
50
100
Temperature (°C)

Figure 6

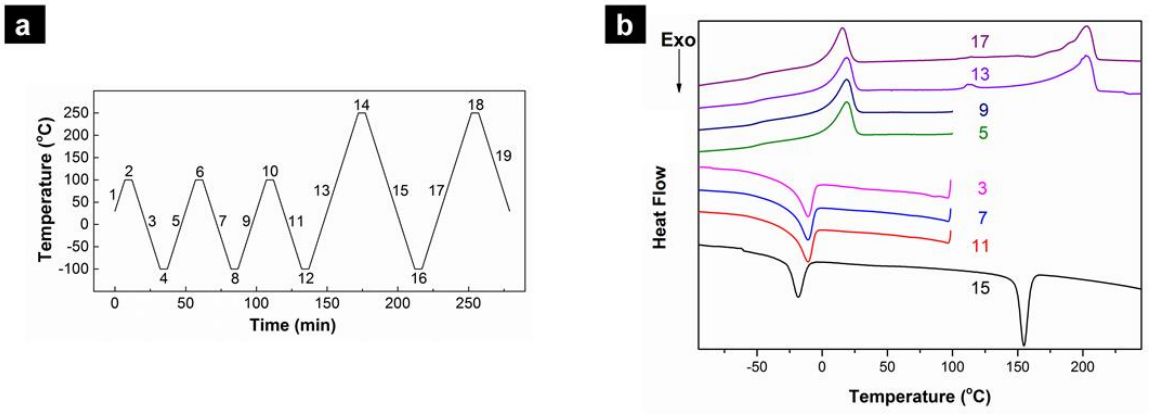

Figure 7

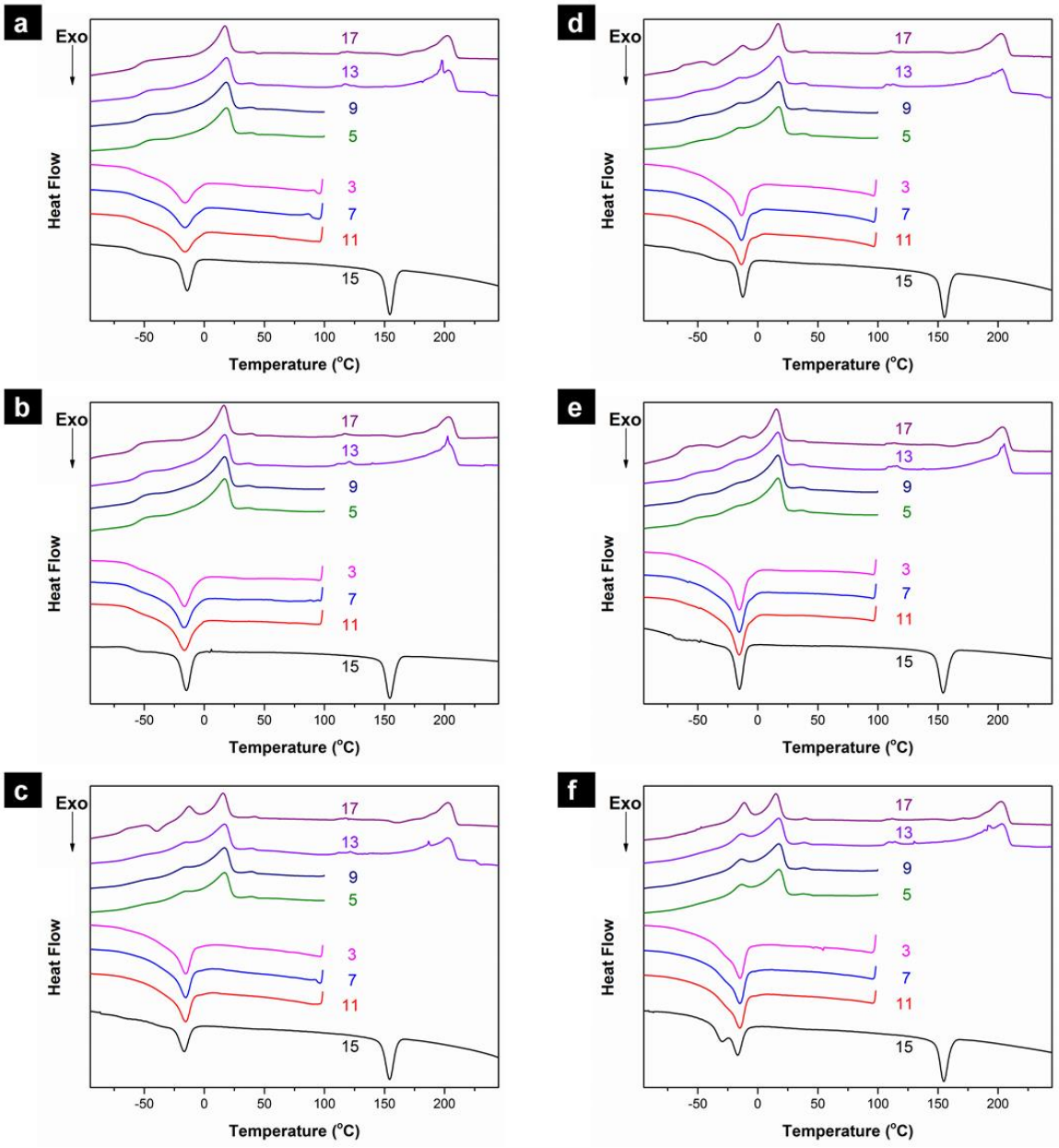
a
b
c
d
e
f
Exo
Heat Flow
Temperature (°C)
17
13
9
5
3
7
11
15
-50
0
50
100
150
200

Figure 8

Table 1

Acronym of product	Definition
PEG-GLY-POSS-Chloroform	PEG modified Glycidyl POSS using Chloroform as solvent
PEG-GDMS-POSS-Chloroform	PEG modified Glycidyldimethylsilyl POSS using Chloroform as solvent
PEG-GLY-POSS-Toluene	PEG modified Glycidyl POSS using Toluene as solvent
PEG-GDMS-POSS-Toluene	PEG modified Glycidyldimethylsilyl POSS using Toluene as solvent
PEG-GLY-POSS-THF	PEG modified Glycidyl POSS using THF as solvent
PEG-GDMS-POSS-THF	PEG modified Glycidyldimethylsilyl POSS using THF as solvent

Table 2

	E_P (kJ/mol)	E_D (kJ/mol)	ΔH_S (kJ/mol)
PEBAX® MH 1657	18.7	31.8	-13.0
PEBAX® MH 1657 + 40% PEG-GLY-POSS Chloroform	16.1	28.3	-12.1
PEBAX® MH 1657 + 40% PEG-GDMS-POSS Chloroform	15.2	26.8	-11.6
PEBAX® MH 1657 + 40% PEG-GLY-POSS Toluene	15.9	28.1	-12.2
PEBAX® MH 1657 + 40% PEG-GDMS-POSS Toluene	14.6	26.3	-11.7
PEBAX® MH 1657 + 40% PEG-GLY-POSS THF	15.4	27.5	-12.1
PEBAX® MH 1657 + 40% PEG-GDMS-POSS THF	14.3	25.9	-11.6

Table 3

	T_g (ºC)					
	PEG-GLY-POSS-Chloroform	PEG-GDMS-POSS-Chloroform	PEG-GLY-POSS-Toluene	PEG-GDMS-POSS-Toluene	PEG-GLY-POSS-THF	PEG-GDMS-POSS-THF
Nanofiller	-59 ±0.1	-67 ± 0.1	-59 ± 0.1	-64 ± 0.4	-69 ± 0.1	-71 ± 0.1
PEBAX® MH 1657 + 40 wt% nanofiller	-54 ± 0.3	-59 ± 0.8	-54 ± 0.6	-58 ± 0.8	-59 ± 1.1	-
PEBAX® MH 1657	-51 ± 0.5					

Supplementary information

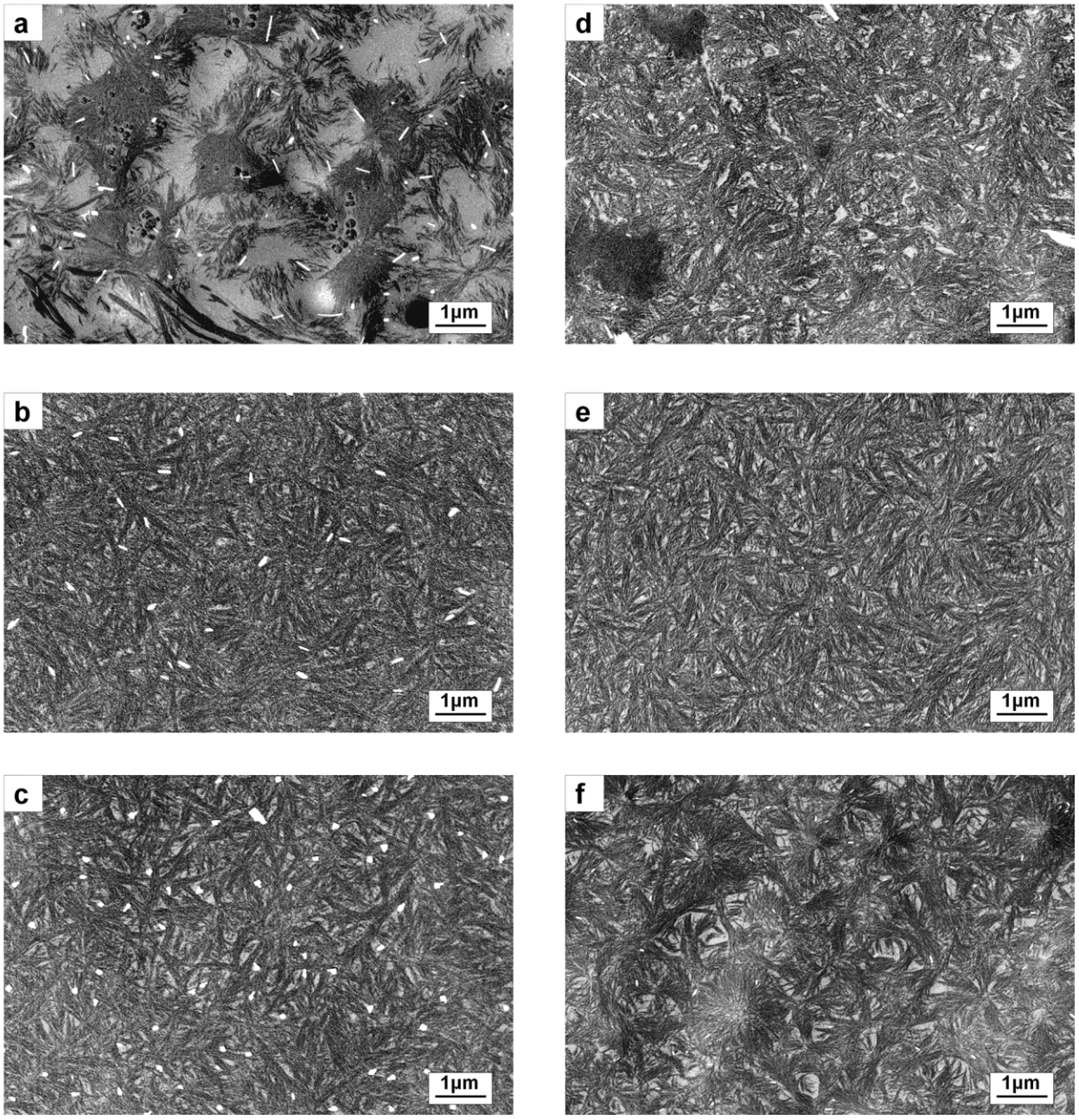

S 1: Surface of the PEBAX® MH 1657 nanocomposites containing 40 wt% – (a) PEG-GLY-POSS-Chloroform (b) PEG-GLY-POSS-Toluene (c) PEG-GLY-POSS-THF (d) PEG-GDMS-POSS-Chloroform (e) PEG-GDMS-POSS-Toluene (f) PEG-GDMS-POSS-THF.

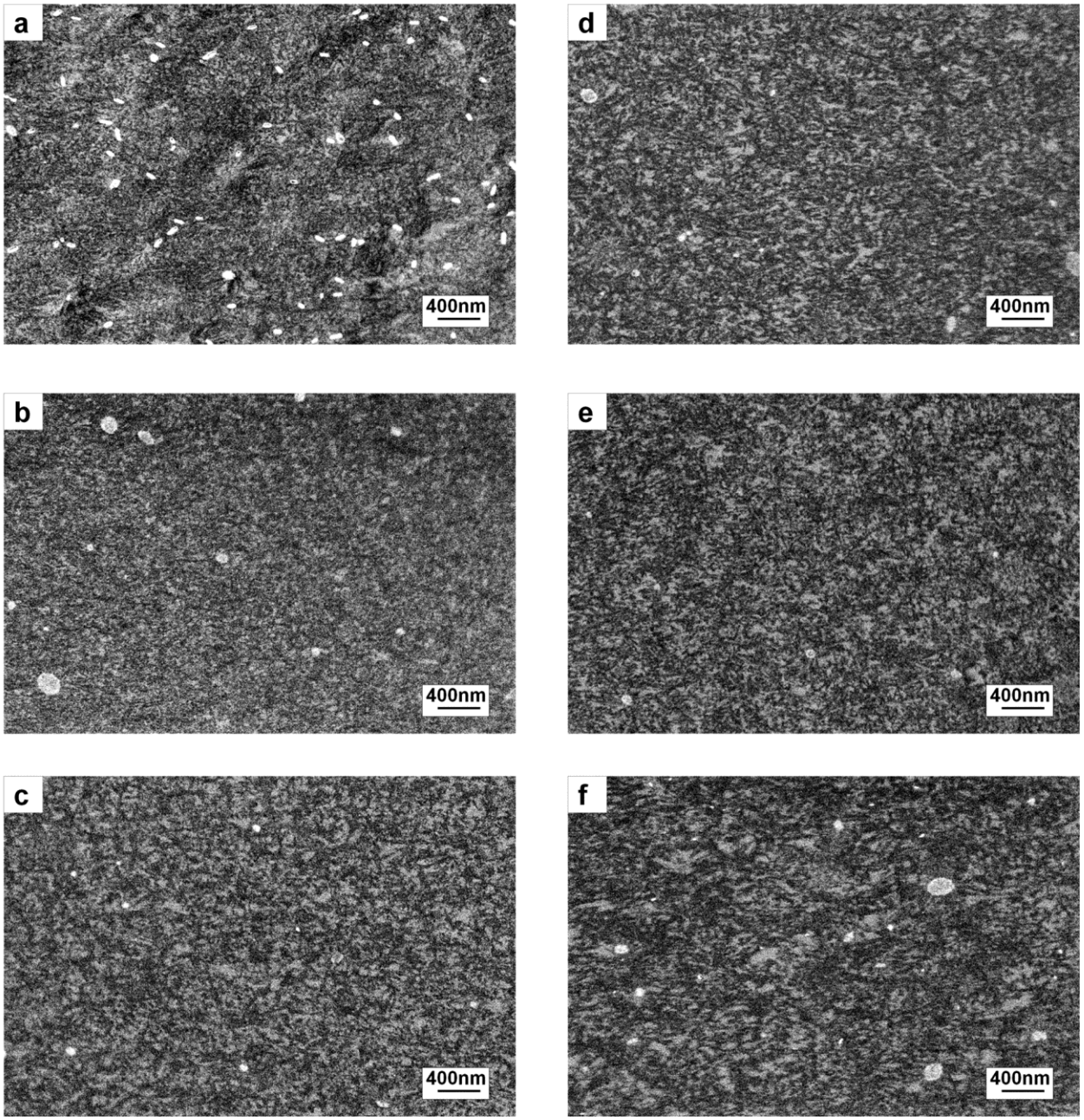

S 2: Cross section of the PEBAX® MH 1657 nanocomposites containing 40 wt% – (a) PEG-GLY-POSS-Chloroform (b) PEG-GLY-POSS-Toluene (c) PEG-GLY-POSS-THF (d) PEG-GDMS-POSS-Chloroform (e) PEG-GDMS-POSS-Toluene (f) PEG-GDMS-POSS-THF.

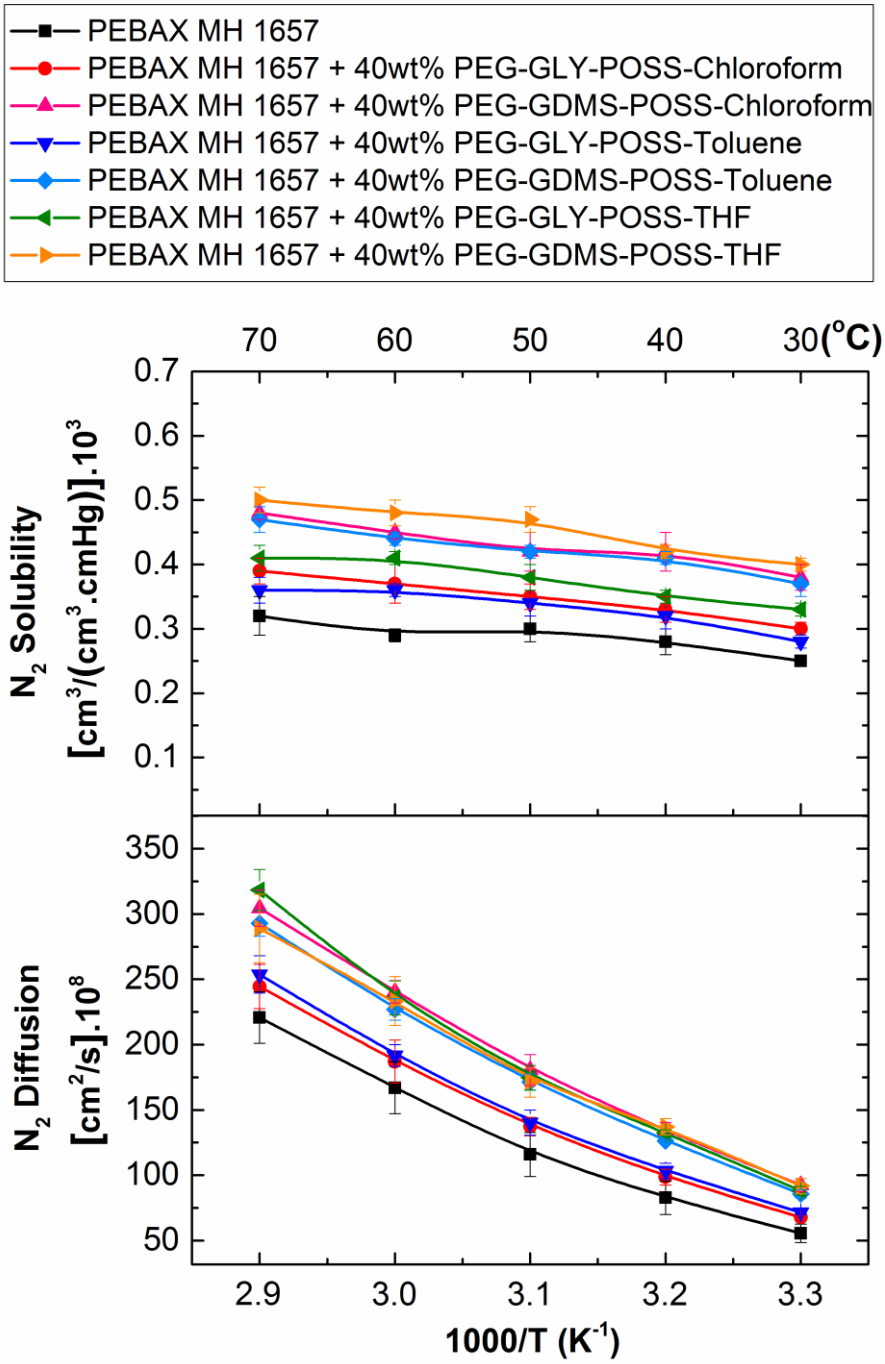

S 3: Diffusion and solubility of N_2 as a function of temperature of PEBAX® MH 1657 and nanocomposites containing 40 wt% nanofiller.

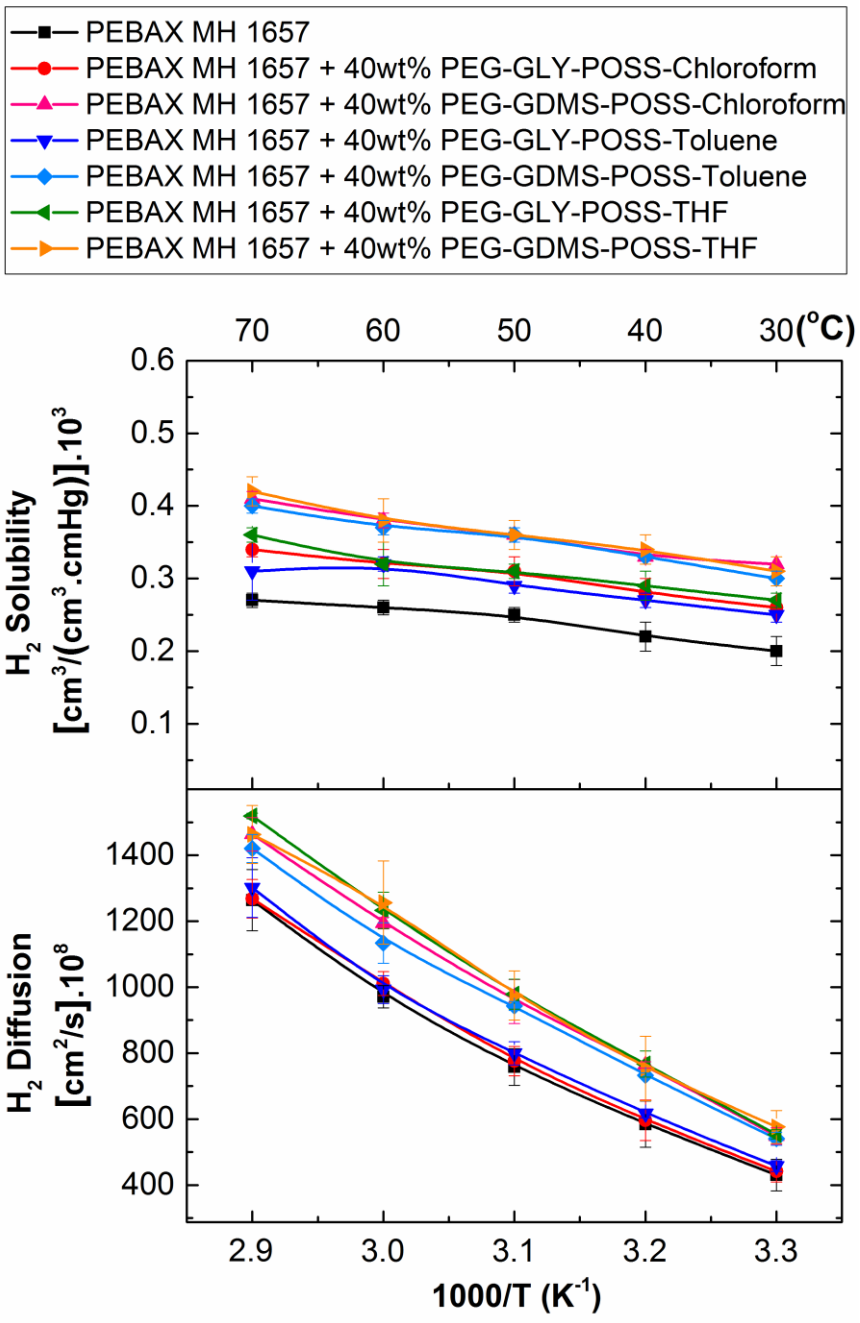

S 4: Diffusion and solubility of H_2 as a function of temperature of PEBAX® MH 1657 and nanocomposites containing 40 wt% nanofiller.

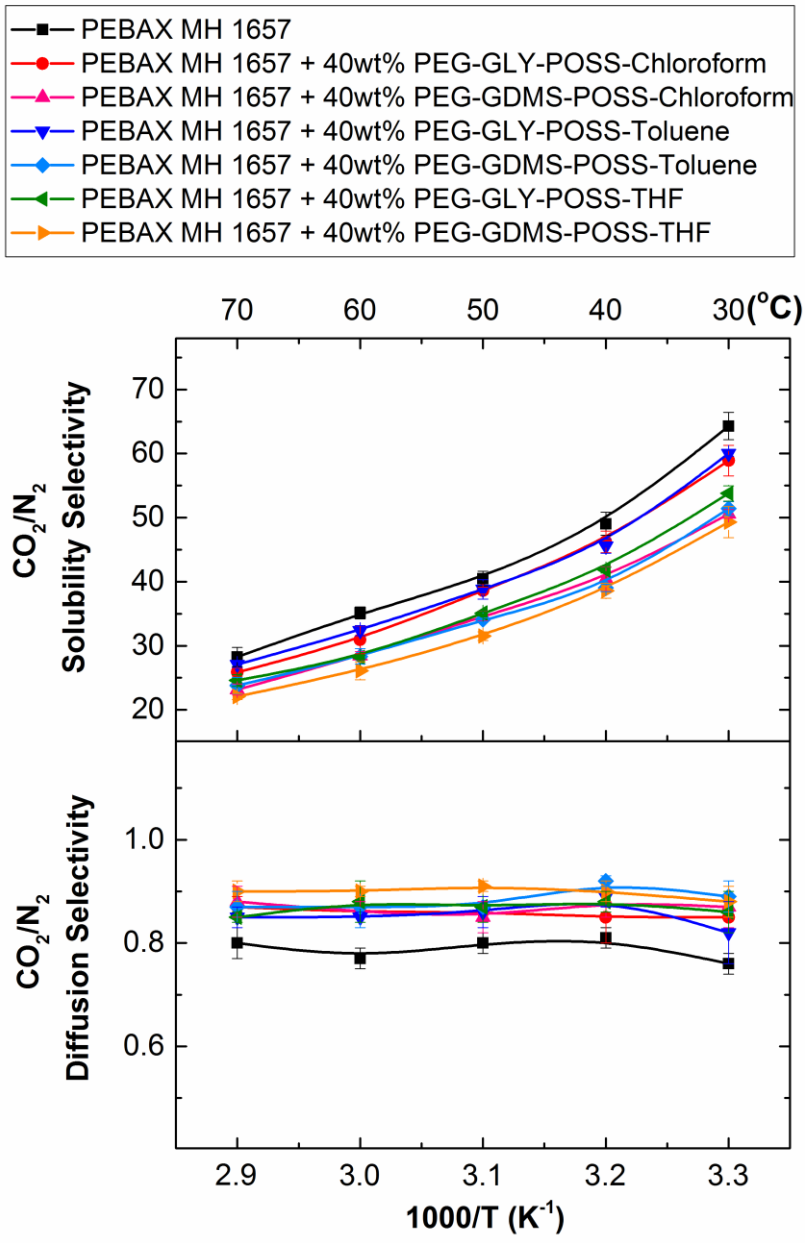

S 5: Diffusion selectivity and solubility selectivity of CO_2 over N_2 as a function of temperature of PEBAX® MH 1657 and nanocomposites containing 40 wt% nanofiller.

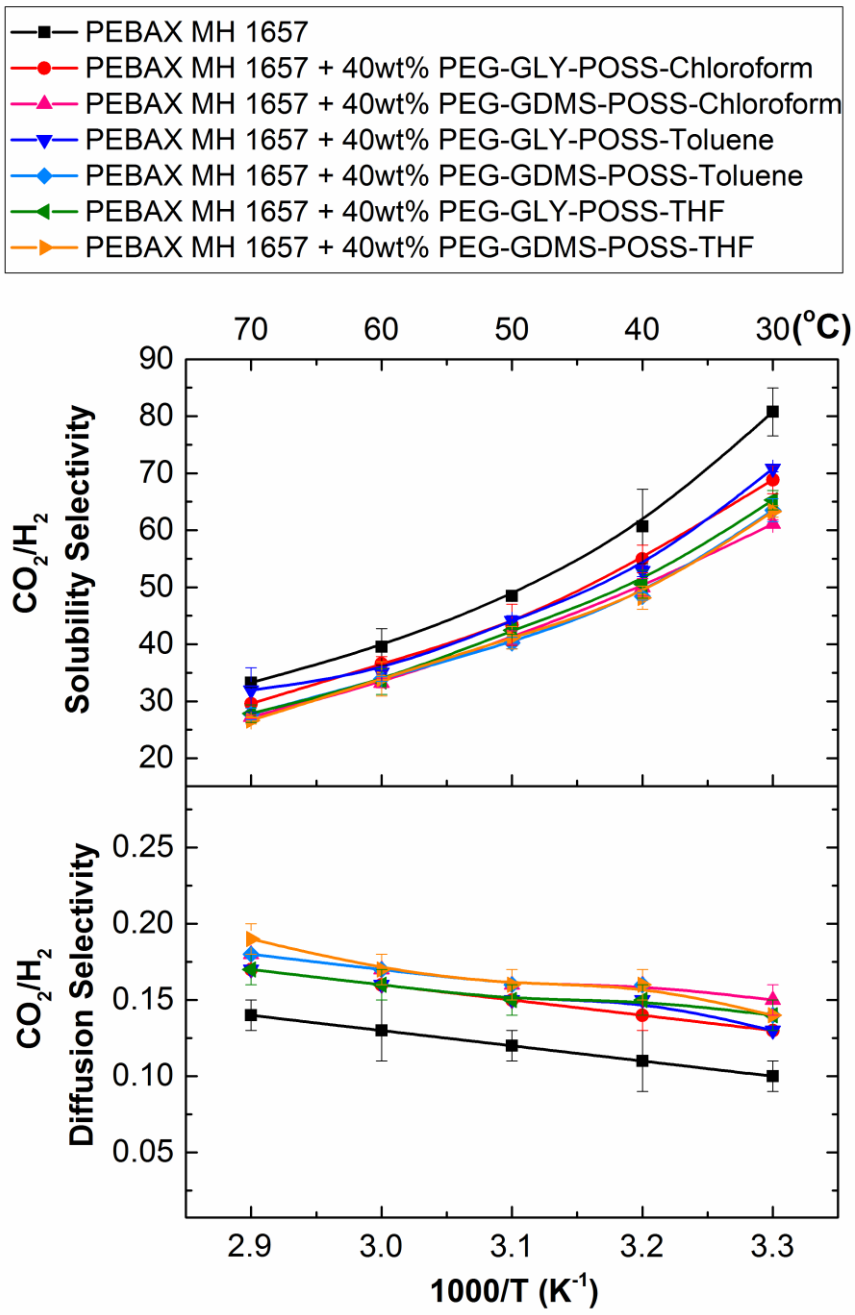

S 6: Diffusion selectivity and solubility selectivity of CO_2 over H_2 as a function of temperature of PEBAX® MH 1657 and nanocomposites containing 40 wt% nanofiller.